Blind identification of the kinetic parameters in three-compartment models

INSTITUTE OF PHYSICS PUBLISHING PHYSICS IN MEDICINE AND BIOLOGY

Phys. Med. Biol. **49** (2004) 639–664 PII: S0031-9155(04)68702-1

Blind identification of the kinetic parameters in three-compartment models

Dmitri Y Riabkov and Edward V R Di Bella

Department of Radiology, University of Utah, 729 Arapeen Dr, Salt Lake City, UT 84108, USA

E-mail: riabkov@ucair.med.utah.edu and ed@ucair.med.utah.edu

Received 3 September 2003
Published 6 February 2004
Online at stacks.iop.org/PMB/49/639 (DOI: 10.1088/0031-9155/49/5/001)

Abstract

Quantified knowledge of tissue kinetic parameters in the regions of the brain and other organs can offer information useful in clinical and research applications. Dynamic medical imaging with injection of radioactive or paramagnetic tracer can be used for this measurement. The kinetics of some widely used tracers such as [^{18}F]2-fluoro-2-deoxy-D-glucose can be described by a three-compartment physiological model. The kinetic parameters of the tissue can be estimated from dynamically acquired images. Feasibility of estimation by blind identification, which does not require knowledge of the blood input, is considered analytically and numerically in this work for the three-compartment type of tissue response. The non-uniqueness of the two-region case for blind identification of kinetic parameters in three-compartment model is shown; at least three regions are needed for the blind identification to be unique. Numerical results for the accuracy of these blind identification methods in different conditions were considered. Both a separable variables least-squares (SLS) approach and an eigenvector-based algorithm for multichannel blind deconvolution approach were used. The latter showed poor accuracy. Modifications for non-uniform time sampling were also developed. Also, another method which uses a model for the blood input was compared. Results for the macroparameter K, which reflects the metabolic rate of glucose usage, using three regions with noise showed comparable accuracy for the separable variables least squares method and for the input model-based method, and slightly worse accuracy for SLS with the non-uniform sampling modification.

1. Introduction

With improvements in medical imaging, tracer kinetic modelling is becoming a powerful tool in the diagnosis and management of cancer, stroke and heart attack. Certain radioactive

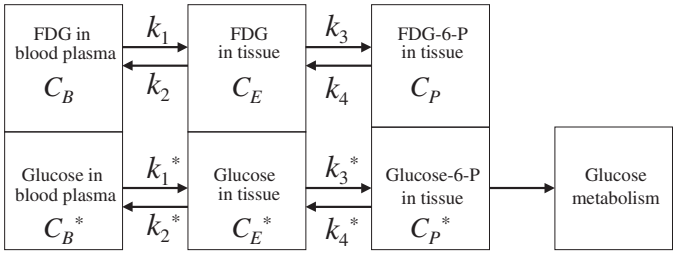

Figure 1. Diagram describing kinetics of FDG and glucose. k_1 and k_2 constants denote rates of the FDG transport from the plasma to the tissue and back, respectively. k_3 and k_4 correspond to the rates of the FDG going to the phosphorylated form and back, respectively. FDG concentration in plasma is denoted as C_B, and the concentration in tissue is denoted as C_E. FDG-6-P concentration is denoted as C_P. The corresponding concentrations and rates of the glucose are denoted in the same way only with a star superscript.

and paramagnetic substances can be used as tracers in dynamic medical imaging to study processes in living tissue. The behaviour of many tracers used in PET (positron emission tomography), SPECT (single photon emission computer tomography) and MRI (magnetic resonance imaging) can be quantitatively approximated by physiological compartment models. Regional knowledge of tissue kinetic parameters in these models can offer information useful in clinical and research applications. Perfusion of tissue (delivery of blood to tissue), washout rates and metabolism are some of the kinetic parameters that can be estimated from a dynamically acquired sequence of images.

This work addresses the three-compartment model used in Huang *et al* (1980). This three-compartment model is appropriate for certain types of tracers, such as glucose labelled with radioactive 18-fluorine, [^{18}F]2-fluoro-2-deoxy-D-glucose (FDG). These labelled glucose tracers are widely used in PET studies of cancer. The three-compartment model can be represented with a diagram describing the kinetics of FDG and glucose in the brain tissue (figure 1, see also Huang *et al* (1980)). The three-compartment model involves four kinetic parameters $\mathbf{k} = [k_1, k_2, k_3, k_4]^T$ which describe regional glucose metabolism (Phelps *et al* 1979). These kinetic parameters can be estimated from a dynamic sequence of images. In PET images single voxel regions typically lack the SNR required for robust fitting to the compartment model. Therefore, regions of interest (ROI) are drawn in the summed images to combine spatially close voxels with similar dynamic curves. Tissue time–activity curves (TACs) are obtained as the activity versus time in each region. The following system of equations:

$$x^{(i)}(t) = (h(\mathbf{k}^{(i)}) \otimes b)(t) + \varepsilon^{(i)}(t) \tag{1}$$

can describe the TACs, where convolution is denoted by $\otimes$, $x^{(i)}$ is the measured TAC for the tissue region i, $h(\mathbf{k}^{(i)}, t)$ is the FDG tissue response for the tissue region i, $b(t)$ is the arterial input function (the tracer available to the tissue for uptake from the blood stream) and $\varepsilon^{(i)}(t)$ is the noise coming from the measurement process (Huang *et al* 1980). In order to estimate the kinetic parameters, the convolution of the measured arterial input function with the FDG tissue response is fitted to the TAC for each region by varying the kinetic parameters in the tissue response. This requires the measurement of the plasma concentration of the tracer. This measurement should be performed accurately and synchronously with imaging, because an accurate input function is critical for unbiased model estimates. Input functions taken from the images, such as using the carotid for brain imaging or the left ventricle for other imaging

can be noisy, and suffer from partial volume effects. It is also not practical to estimate the plasma portion, which is needed for the input function since only the tracer in the plasma is available to the tissues.

New methods of estimation, however, have begun to appear since the blood input measurement is invasive and difficult (Feng *et al* 1997, DiBella *et al* 1999]. The subject of many works has been less invasive techniques (population-based approaches (Takikawa *et al* 1993), venous sampling (Chen *et al* 1998)). Another type of techniques, termed blind identification methods, has begun to be developed recently for three-compartment (Feng *et al* 1997, Wong *et al* 2001, Riabkov and DiBella 2002b) and two-compartment (DiBella *et al* 1999, Riabkov and DiBella 2002a) models. These methods do not require any knowledge of the blood input and are based on the fact that multiple tissue regions or 'channels' are driven by the same input function. (TACs for different regions are the responses with different parameters convolved with the same input.) The relative values of the k_1 parameters can be estimated by the blind methods. However, the absolute values can be obtained from the relative values by using one venous sample at a late time when arterial and venous concentrations are the same. This sample can be used to determine the global scale factor.

An empirical approach has been used in most works to date for testing the blind methods (Feng *et al* 1997, DiBella *et al* 1999, Wong *et al* 2001, Riabkov and DiBella 2002a). However, the blind identification problem solution is influenced by many factors. A certain condition, for example, should be satisfied for this system of equations to be solvable. That is, the transfer functions $h^{(i)}(t)$ of different channels should be linearly independent. (It is possible to have some common poles or zeros in different channels but not all of them should be common.) The degree of closeness of zeros or poles in the different channels as well as the noise level will influence the accuracy of the solution (Riabkov and DiBella 2002a). Therefore, many different sets of data are needed in the numerical approach applied to this problem to get proper validation of the numerical technique.

This work investigates the three-compartment system analytically as well as numerically. Using analytical methods, the question of uniqueness of blind identification of $\mathbf{k}$ for a three-compartment model is addressed. The question of uniqueness of the solution is whether only one set of $\mathbf{k}^{(i)}$ and blood input function b corresponds to the set of $x^{(i)}$ of the measured TACs. In this work it is shown that if only two regions are used, the solution is not unique. More regions are shown to lead to a unique solution within a global scale factor. Also, the accuracy of the estimations by versions of the blind identification methods EVAM (eigenvector based algorithm for multichannel blind deconvolution) (Gürelli and Nikias 1995), SLS (separable variables least squares) (Golub and Pereyra 1973) which is a more general version of IQML (iterative quadratic maximum likelihood) (Bresler and Macovski 1986) and a TACs modelling method similar to (Feng *et al* 1997, Wong *et al* 2001) were investigated numerically.

Blind methods applied to the physiological systems can be divided into two categories. One is pure blind identification which can be used with no assumptions about the blood input function (DiBella *et al* 1999, Riabkov and DiBella 2002a). Another is to assume that the unknown blood input fits a certain modelling function dependent on a few parameters (Feng *et al* 1997, Wong *et al* 2001). One disadvantage of the latter approach is that extensive knowledge of the blood curves from many patients is required in order for an accurate function model to be created. Inaccuracy of the input model will lead to errors in the estimates of the kinetic parameters.

This work shows that a disadvantage of the pure blind identification approaches (Riabkov and DiBella 2002a) for the three-compartment system is that they can give slightly less accurate kinetic estimates than the modelling method. One advantage is that no knowledge of the blood input or extensive database of the blood curves is required. Another advantage

is that the errors in the estimates of kinetic parameters due to the inaccuracy of input model function will not be introduced.

2. Blind identification methods

In this work the eigenvector-based algorithm for multichannel blind deconvolution (Gürelli and Nikias 1995) and separable variables least squares (Golub and Pereyra 1973) which is a more general version of iterative quadratic maximum likelihood (Tong and Perreau 1998) blind identification methods were used. The descriptions for these methods adapted for a two-compartment model can be found in Riabkov and DiBella (2002a).

IQML is based on minimizing the objective function

$$\|\mathbf{x} - \mathbf{H}\mathbf{b}\|^2 \tag{2}$$

where $\mathbf{H}$ are convolution matrices that are functions of the kinetic parameters and $\mathbf{b}$ here is the least-squares solution to the linear system $\mathbf{x} = \mathbf{H}\mathbf{b}$ at each estimate of $\mathbf{H}$. The kinetic parameter estimates are found at the minimum of this function.

For the SLS method, the only change from the IQML method used in Riabkov and DiBella (2002a) that is needed due to the transition to the three compartments is that the matrix $\mathbf{H}$ is constructed from three-compartmental tissue responses which are dependent on $\mathbf{k}$ parameters (here we call the method SLS rather than IQML because the noise model is no longer white Gaussian). Everything is the same, only the $\mathbf{k}$ are used instead of k_I, k_O. The requirement on the tissue responses for SLS is that the tissue responses have to be linearly independent (otherwise SLS would try to converge to the solution where the matrix $\mathbf{H}$ is singular, which would not be possible). This means that the sets of k_2, k_3, k_4 parameters in the different channels should not be the same. Therefore to satisfy this condition the ROIs should be chosen such that the shapes of the TACs are different.

EVAM is based on the construction of a filter for each of the channels, the outputs of which are equalized by varying parameters of the filters, which are functions of the kinetic parameters. The changes in the EVAM case from the two-compartment model to the three-compartment model are considered in the following sections.

3. Three-compartmental tissue response analysis with EVAM

The goal is to estimate the kinetic parameters of the tissue in multiple distinct tissue regions (channels).

Assume that the signals are sampled at times $t_n = n\Delta t$, where $n = 0, \ldots, N-1$, and that we have two channels.

Consider the following task. An elegant analytical approach (Gürelli and Nikias 1995) to the analysis of this system requires construction of a finite impulse response (FIR) filter (see Proakis and Manolakis (1996)) for each of two channels such that the outputs of these two filters would be the same. Denote the filter input signals as $x^{(i)}(n)$ where i is the channel (or filter) index. Denote filter i as $w^{(i)}(m)$ and $w_m^{(i)}$ are the coefficients of the FIR filter (see Proakis and Manolakis (1996)) where $m = 0, \ldots, W^{(i)}$, where $W^{(i)}$ is the order of the filter. This task can be done by minimization of Euclidean distance between the two outputs, and the coefficients of the FIR filters are the variables of this minimization. As a result of this minimization, the coefficients are determined which determines also the FIR filters.

The two different TACs drawn from the two ROIs of the same dynamic sequence of images present the same blood input convolved with two different tissue responses. The set of the tissue kinetic parameters for each ROI determines each tissue response function. It will

be shown that if the two filter signal inputs are the two different TACs, then the coefficients of the FIR filters (in this case the orders $W^{(i)}$ of the FIR filters will be all equal to some number M, which is defined by the form of the tissue response) can be directly represented in terms of tissue kinetic parameters and vice versa. The goal is the estimation of the kinetic parameters. These filter coefficients will provide the kinetic parameter estimates. While this estimation provides unique parameters in the two-compartment model case (Riabkov and DiBella 2002a), the analysis of the tissue response in this section shows that this representation is not unique for the three-compartment model case, when only two tissue regions are used.

The EVAM cost function is the square of the Euclidean distance between the outputs of the two FIR filters.

$$\mathcal{E}(\mathbf{w}) = \sum_n ((x^{(i)} \otimes w^{(i)})(n) - (x^{(j)} \otimes w^{(j)})(n))^2 \tag{3}$$

here vector $\mathbf{w} = [\mathbf{w}^{(i)T}, \mathbf{w}^{(j)T}]^T$, where $\mathbf{w}^{(i)T} = \left[w_0^{(i)}, w_1^{(i)}, \ldots, w_M^{(i)}\right]$, and $\mathbf{w}^{(j)T} = \left[w_0^{(j)}, w_1^{(j)}, \ldots, w_M^{(j)}\right]$. Close consideration of the expression for the Euclidean distance between the outputs of two FIRs has shown that the FIR coefficients minimizing this distance would be the elements of the eigenvector corresponding to the minimal eigenvalue of a certain correlation matrix $\mathbf{R}$ (Riabkov and DiBella 2002a, Gürelli and Nikias 1995). This matrix is formed from two TAC signals in the following way:

$$\mathbf{R} = \begin{bmatrix} \mathbf{R}_{1,1} & -\mathbf{R}_{1,2} \\ -\mathbf{R}_{2,1} & \mathbf{R}_{2,2} \end{bmatrix} \tag{4}$$

and the block matrices are defined as

$$\mathbf{R}_{i,j} = \sum_{n=M}^{N} \mathbf{x}^{(i)}(n)\mathbf{x}^{(j)T}(n) \tag{5}$$

where $\mathbf{x}^{(i)}(n) = [x^{(i)}(n), x^{(i)}(n-1), \ldots, x^{(i)}(n-M)]^T$.

Since convolution operations are involved it is most convenient to consider the signals in the z-domain. (The definition of the z-transform can be found in Proakis and Manolakis (1996).) The z-transforms of $x^{(i)}$ and $b(n)$ are $\mathcal{X}^{(i)}(z)$ and $\mathcal{B}(z)$. The convolution $x^{(i)}(n) = (b \otimes h^{(i)})(n)$ is multiplication in the z-domain $\mathcal{X}^{(i)}(z) = \mathcal{B}(z)\mathcal{H}^{(i)}(z)$, where $\mathcal{H}^{(i)}(z)$ is the z-transform of the tissue response $h^{(i)}(n)$. Also the z-transform of $w^{(i)}(m)$ is $\mathcal{W}^{(i)}(z)$. Therefore the EVAM cost function $\mathcal{E}(\mathbf{w})$ is proportional to

$$\mathcal{X}^{(i)}(z)\mathcal{W}^{(i)}(z) - \mathcal{X}^{(j)}(z)\mathcal{W}^{(j)}(z) = \mathcal{B}(z)(\mathcal{H}^{(i)}(z)\mathcal{W}^{(i)}(z) - \mathcal{H}^{(j)}(z)\mathcal{W}^{(j)}(z)). \tag{6}$$

The tissue response for FDG (Phelps *et al* 1979) can be written as

$$h(t) = B_1 \,\mathrm{e}^{-a_1 t} - B_2 \,\mathrm{e}^{-a_2 t} \tag{7}$$

where

$$B_i = \frac{k_1}{q}(k_3 + k_4 - a_i) \qquad i = 1, 2 \tag{8}$$

$$a_1 = \frac{k_2 + k_3 + k_4 - q}{2} \tag{9}$$

$$a_2 = \frac{k_2 + k_3 + k_4 + q}{2} \tag{10}$$

$$q = \sqrt{(k_2 + k_3 + k_4)^2 - 4k_2k_4}. \tag{11}$$

Then the transfer function for a channel is equal to

$$\mathcal{H}(z) = \frac{B_1}{1 - \mathrm{e}^{-a_1 \Delta t} z^{-1}} - \frac{B_2}{1 - \mathrm{e}^{-a_2 \Delta t} z^{-1}} \tag{12}$$

We will denote the two exponential factors as

$$u = \mathrm{e}^{-a_1 \Delta t} \qquad v = \mathrm{e}^{-a_2 \Delta t}. \tag{13}$$

Let

$$\mathcal{H}(z) = \frac{\mathcal{C}(z)}{\mathcal{D}(z)} \tag{14}$$

where $\mathcal{C}(z)$ and $\mathcal{D}(z)$ are FIRs. In other words $\mathcal{C}(z)$ and $\mathcal{D}(z)$ are polynomials of orders C and D with coefficients $c_0, \ldots, c_C$ and $d_0, \ldots, d_D$ correspondingly,

$$\mathcal{C}(z) = c_0 + c_1 z^{-1} + \cdots + c_C z^{-C}$$
$$\mathcal{D}(z) = d_0 + d_1 z^{-1} + \cdots + d_D z^{-D}.$$

The numerator is given by

$$\mathcal{C}(z) = B_1 - B_2 + \frac{-B_1 v + B_2 u}{z}$$

where from (8) we have

$$B_1 - B_2 = \frac{k_1}{q}(-a_1 + a_2).$$

Also from (9) and (10)

$$q = -a_1 + a_2$$

then

$$B_1 - B_2 = k_1 \tag{15}$$

and thus $\mathcal{C}(z)$ and $\mathcal{D}(z)$ take on the forms

$$\mathcal{C}(z) = k_1 + \frac{-B_1 v + B_2 u}{z} \tag{16}$$

$$\mathcal{D}(z) = 1 + \frac{-u - v}{z} + \frac{uv}{z^2}. \tag{17}$$

Therefore the orders C and D are 1 and 2, respectively. And the coefficients of the $\mathcal{D}(z)$ and $\mathcal{C}(z)$ are

$$c_0 = k_1 \qquad c_1 = -B_1 v + B_2 u \tag{18}$$

$$d_0 = 1 \qquad d_1 = -u - v \tag{19}$$

$$d_2 = uv. \tag{20}$$

And we have

$$\mathcal{C}(z) = k_1 z^{-1}(z - s) \tag{21}$$

$$\mathcal{D}(z) = z^{-2}(z - u)(z - v) \tag{22}$$

where the new variable s is given by

$$s = -\frac{c_1}{k_1}. \tag{23}$$

Let i and j be two distinct channels ($i \neq j$). As in Riabkov and DiBella (2002a) it is assumed that the transfer functions of the tissue responses for different channels (regions) do not have any common zeros or poles (termed here the *identifiability condition*). As was mentioned, the EVAM cost function $\mathcal{E}(\mathbf{w})$ is proportional to

$$\mathcal{E}(\mathbf{w}) \sim (\mathcal{H}^{(i)}\mathcal{W}^{(i)} - \mathcal{H}^{(j)}\mathcal{W}^{(j)}). \tag{24}$$

Also let us assume that $\mathcal{W}^{(i)}$ and $\mathcal{W}^{(j)}$ are FIR filters with orders

$$W^{(i)} = C^{(j)} + D^{(i)} \qquad W^{(j)} = C^{(i)} + D^{(j)}. \tag{25}$$

Then, substituting $\mathcal{H}$ and assuming the noise-free case, the minimum of the cost function is achieved at

$$\frac{z(z - s^{(i)})k_1^{(i)}\mathcal{W}^{(i)}}{(z - u^{(i)})(z - v^{(i)})} - \frac{z(z - s^{(j)})k_1^{(j)}\mathcal{W}^{(j)}}{(z - u^{(j)})(z - v^{(j)})} = 0. \tag{26}$$

It can be seen that because of *identifiability* assumption (that the transfer functions do not have common poles and zeros), the only solutions for the $\mathcal{W}$ minimizing $\mathcal{E}(\mathbf{w})$ are

$$\mathcal{W}^{(i)}(z) = \alpha\mathcal{C}^{(j)}(z)\mathcal{D}^{(i)}(z) \qquad \mathcal{W}^{(j)}(z) = \alpha\mathcal{C}^{(i)}(z)\mathcal{D}^{(j)}(z) \tag{27}$$

where α is an arbitrary constant. Therefore the FIR filter for blind deconvolution that will minimize (3), $\mathcal{W}(z)$, is given by

$$\mathcal{W}^{(i)}(z) = \alpha k_1^{(j)} \left(1 - \frac{s^{(j)}}{z}\right)\left(1 - \frac{u^{(i)}}{z}\right)\left(1 - \frac{v^{(i)}}{z}\right). \tag{28}$$

The coefficients of the polynomial $\mathcal{W}^{(i)}(z)$ are

$$\begin{cases} w_0^{(i)} = \alpha k_1^{(j)} \\ w_1^{(i)} = \alpha k_1^{(j)}(-u^{(i)} - v^{(i)} - s^{(j)}) \\ w_2^{(i)} = \alpha k_1^{(j)}(u^{(i)}v^{(i)} + u^{(i)}s^{(j)} + v^{(i)}s^{(j)}) \\ w_3^{(i)} = \alpha k_1^{(j)}(-u^{(i)}v^{(i)}s^{(j)}). \end{cases} \tag{29}$$

The following constants can be calculated from the coefficients of $\mathcal{W}(z)$

$$n_1 = \frac{w_1}{w_0} \qquad n_2 = \frac{w_2}{w_0} \qquad n_3 = \frac{w_3}{w_0} \tag{30}$$

for both i and j. Then the following system can be written as:

$$\begin{cases} n_1^{(i)} = -u^{(i)} - v^{(i)} - s^{(j)} \\ n_2^{(i)} = u^{(i)}v^{(i)} + u^{(i)}s^{(j)} + v^{(i)}s^{(j)} \\ n_3^{(i)} = -u^{(i)}v^{(i)}s^{(j)}. \end{cases} \tag{31}$$

It should be noted that $u^{(i)}$, $v^{(i)}$ and $s^{(j)}$ are the roots of the polynomial constructed from $n_1^{(i)}, n_2^{(i)}, n_3^{(i)}$:

$$\begin{aligned} p^{(i)}(z) &= (z - u^{(i)})(z - v^{(i)})(z - s^{(j)}) \\ &= z^3 + n_1^{(i)}z^2 + n_2^{(i)}z + n_3^{(i)} \end{aligned} \tag{32}$$

and also that $u^{(j)}$, $v^{(j)}$ and $s^{(i)}$ are the roots of the polynomial

$$\begin{aligned} p^{(j)}(z) &= (z - u^{(j)})(z - v^{(j)})(z - s^{(i)}) \\ &= z^3 + n_1^{(j)}z^2 + n_2^{(j)}z + n_3^{(j)}. \end{aligned} \tag{33}$$

Since the w coefficients can be found as the eigenvector corresponding to the minimal eigenvalue of the matrix $\mathbf{R}$ which is constructed from the TACs data (4), values n can be calculated from w (30). Polynomials $p(z)$ are constructed from n, therefore u, v and s can be calculated as the roots of these polynomials (see appendix A.1).

3.1. Kinetic parameters

The parameters $k_2^{(i)}, k_3^{(i)}, k_4^{(i)}$ can be expressed in terms of $u^{(i)}$, $v^{(i)}$ and $s^{(i)}$. (Note that u, v and s should be for the same channel, unlike the above derivation, for example (32). In view of this uniformity the superscript $^{(i)}$ denoting the channel number is omitted in the formulae below.)

$$k_4 = \frac{a_2 a_1}{k_2} \tag{34}$$

$$k_3 = -k_2 + (a_1 + a_2) - \frac{a_2 a_1}{k_2} \tag{35}$$

$$k_2 = \frac{-s(a_2 - a_1) + v a_2 - u a_1}{v - u}. \tag{36}$$

The proof of these expressions is given in appendix A.2. Because of (13), we have

$$a_1 = -\frac{\ln(u)}{\Delta t} \qquad a_2 = -\frac{\ln(v)}{\Delta t}. \tag{37}$$

Also, it can be seen from (36) that the coefficients k_4, k_3 and k_2 do not depend on the arbitrary constant α.

3.2. Tissue response

Another advantage of using the u, v, s notation is that the tissue response expressed in terms of u, v, s is less complex than expression (7) written in terms of k_2, k_3, k_4:

$$h(n) = \Delta t \frac{k_1}{u - v}((u - s)u^n + (s - v)v^n). \tag{38}$$

This expression is derived in appendix A.3. (The Δt factor is needed for discrete convolution to be equal to continuous convolution.)

3.3. Constraints

It can be shown that if all rates $k_1, k_2, k_3, k_4 > 0$ then

$$0 < v < s < u < 1. \tag{39}$$

The proof of this expression is shown in appendix A.4.

3.4. Uniqueness

Let us denote two vectors

$$\mathbf{\Phi}^{(i,j)} = [u^{(i)}, v^{(i)}, s^{(j)}]^T \qquad \mathbf{\Phi}^{(j,i)} = [u^{(j)}, v^{(j)}, s^{(i)}]^T.$$

Suppose we found three roots $r_1^{(i)}, r_2^{(i)}, r_3^{(i)}$ of the $p^{(i)}(z)$ (see appendix A.1). One of these three roots corresponds to $u^{(i)}$, another one to $v^{(i)}$ and the other to $s^{(j)}$. However there is no way to tell which of them corresponds to which. Therefore we have six possible solutions for $\mathbf{\Phi}^{(i,j)}$ resulting from all the permutations of the elements of the vector $\left[r_1^{(i)}, r_2^{(i)}, r_3^{(i)}\right]^T$, and also six possible solutions for $\mathbf{\Phi}^{(j,i)}$ resulting from all the permutations of $\left[r_1^{(j)}, r_2^{(j)}, r_3^{(j)}\right]^T$.

It can be seen from (34)–(36) that if u is interchanged with v then the values of k_2, k_3, k_4 will still be the same. Therefore u and v can be interchanged in $\mathbf{\Phi}$ when calculating k_2, k_3, k_4 from $\mathbf{\Phi}$. Because of this invariance the number of $\left[r_1^{(i)}, r_2^{(i)}, r_3^{(i)}\right]^T$ permutations for the solution

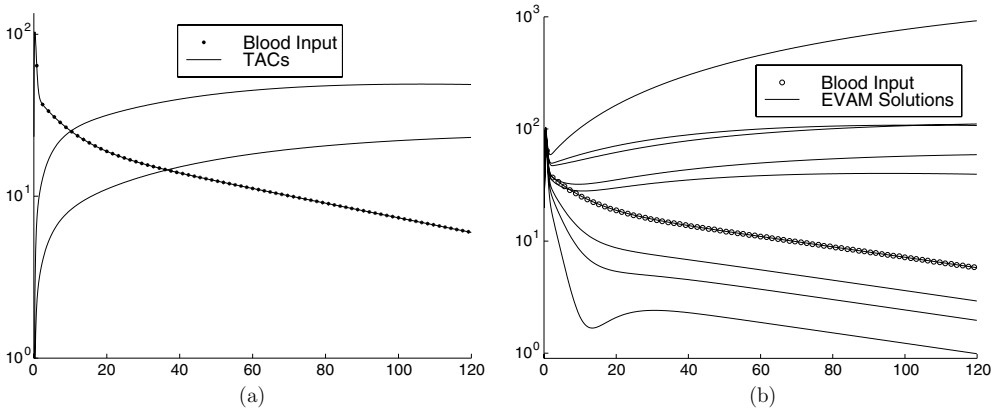

Figure 2. (a) Blood input function (connected dots) and two TACs (activity in μCi/ml versus time in minutes). (b) Nine EVAM blood input solutions.

$\mathbf{\Phi}^{(i,j)}$ as well as the number of $\left[r_1^{(j)}, r_2^{(j)}, r_3^{(j)}\right]^T$ permutations for the solution $\mathbf{\Phi}^{(j,i)}$ that have to be considered for calculation of k_2, k_3, k_4 is three instead of six.

Assume in the two-channel case that we built the $\mathbf{R}$ matrix from the TACs data (see Riabkov and DiBella (2002a)—in three-compartment model case, $W^{(i)} = W^{(j)} = M = 3$) and calculated the roots $r_1^{(i)}, r_2^{(i)}, r_3^{(i)}$ for channel i and the roots $r_1^{(j)}, r_2^{(j)}, r_3^{(j)}$ for the channel j (see appendix A.1). It is possible to use any of the three values $r_1^{(i)}, r_2^{(i)}, r_3^{(i)}$ as $s^{(j)}$ and the two remaining as $u^{(i)}$ and $v^{(i)}$. And independently, it is possible to use any of the three values $r_1^{(j)}, r_2^{(j)}, r_3^{(j)}$ as $s^{(i)}$ and the two remaining as $u^{(j)}$ and $v^{(j)}$. Therefore nine different sets $\{u^{(i)}, v^{(i)}, s^{(i)}, u^{(j)}, v^{(j)}, s^{(j)}\}$ can be formed. As was shown in section 3.1, the parameters $k_2^{(i)}, k_3^{(i)}, k_4^{(i)}$ can be calculated from $u^{(i)}, v^{(i)}, s^{(i)}$ and $k_2^{(j)}, k_3^{(j)}, k_4^{(j)}$ from $u^{(j)}, v^{(j)}, s^{(j)}$. Therefore the two-channel case blind identification problem has nine solutions for the set of parameters, $\mathbf{k}^{(i)}, \mathbf{k}^{(j)}$, and only one solution of these nine corresponds to the true set. This lack of a unique solution means that not only EVAM will fail to choose consistently the correct solution from noise-free data; any method used to estimate the parameters blindly may give incorrect solutions. Note that even if constraint (39) is applied to find the true solution among those nine, there may still be cases where the true solution cannot be identified. In the three-channel case however the solution is unique (see sections 4 and 5.1.1).

3.5. Simulated example

To show numerically that as many as nine different solutions for two-channel blind identification can exist, a simulation was used. Two TAC curves typical for FDG brain imaging were simulated by two tissue responses generated using two sets of physiologically possible $\mathbf{k}$ convolved with a blood input function (figure 2(a)) generated using an empirical formula (Feng *et al* 1997). Then matrix $\mathbf{R}$ (Riabkov and DiBella 2002a) was built from the TACs data (in the three-compartment model case $W^{(i)} = W^{(j)} = M = 3$), and $\mathbf{w}$ was calculated from $\mathbf{R}$ (see Riabkov and DiBella (2002a)). From $\mathbf{w}$ the three roots (49)–(51) for each channel giving were obtained. Three cases in one channel when one of the three roots was assigned to s and the other two were assigned to u and v combined independently with three cases for the other channel, giving nine different solutions of the two $\mathbf{k}$ sets. Only one solution coincided with the original $\mathbf{k}$ sets. The nine sets (of two tissue responses each) correspondent to the nine solutions were then used to deconvolve the two original TACs. (Deconvolution

was performed by using a function 'filter' in Matlab 5.) For all nine cases, the two resulting curves in each set were exactly the same. These nine cases of two coincident curves are shown in figure 2(b).

4. Three-channel case

Consider the common quadratic error for p channels when blood input $\mathbf{b}$ is known

$$\mathcal{E}(\mathbf{k}^{(1)}, \ldots, \mathbf{k}^{(p)}, \mathbf{b}) = \sum_{i=1}^{p} \mathcal{E}(\mathbf{k}^{(i)}, \mathbf{b}) \tag{40}$$

where the error for one channel i is the quadratic difference between the measured and modelled data

$$\mathcal{E}^{(i)} = \mathcal{E}(\mathbf{k}^{(i)}, \mathbf{b}) = \|x^{(i)}(t) - (h(\mathbf{k}^{(i)}) \otimes b)(t)\|^2. \tag{41}$$

The same error function is minimized in the blind identification, except $\mathbf{b} = \mathbf{b}(\mathbf{k}^{(1)}, \ldots, \mathbf{k}^{(p)})$ is an implicit function of the parameters $\mathbf{k}^{(i)}$ of all of the channels. Then for blind identification each channel residual $\mathcal{E}^{(i)}$ and therefore the common error as well are dependent only on all of the $\mathbf{k}^{(1)}, \ldots, \mathbf{k}^{(p)}$ estimates. The two-channel blind identification error function

$$\mathcal{E}(\mathbf{k}^{(1)}, \mathbf{k}^{(2)}) = \mathcal{E}^{(1)} + \mathcal{E}^{(2)} \tag{42}$$

can have nine minima, all equal to zero in the noiseless case, because the blind identification problem has nine solutions in this case. There exist three different pairs of channels among the three channels. As a result, in the three-channel case

$$\mathcal{E}(\mathbf{k}^{(1)}, \mathbf{k}^{(2)}, \mathbf{k}^{(3)}) = \mathcal{E}^{(1)} + \mathcal{E}^{(2)} + \mathcal{E}^{(3)} \tag{43}$$

the error function can have 27 minima, since each pair can give nine local minima. Considering pairwise combinations of the channels, for example, the pairs 1–2 and 1–3, and the parts of the solutions belonging only to the channel 1, any one of the parts of the nine solutions for the pair 1–2 is unlikely to coincide with any one of the channel 1 parts of the nine solutions for the pair 1–3 unless it is the true solution. The same consideration holds for the other channel combinations. Therefore only when $\mathbf{k}^{(1)}, \mathbf{k}^{(2)}, \mathbf{k}^{(3)}$ are equal (or close in the noisy case) to the true parameter set, will the global minimum be reached. (This is only true if the *identifiability condition* holds.)

Note that the minima of the described residuals correspond to the minima of the blind identification cost functions (EVAM or SLS), since they were designed for minimization of these residuals. (The SLS cost function is similar to equation (41), but instead of b the least-squares estimate of b, which is a function of $\mathbf{k}^{(i)}$, is used (Riabkov and DiBella 2002a).) Uniqueness is not shown rigorously; however, numerically EVAM and SLS converge to the true solution (see section 5) for the three-channel case.

5. Numerical analysis

The three-channel case is considered to compare the accuracy of the unique solution in noise by different methods for blind identification when using a three-compartment model.

5.1. Estimation algorithms

The direct calculations of the roots for calculation of the kinetic parameters are not robust in the presence of noise. In noisy conditions, the roots will have non-zero imaginary parts.

To force the imaginary part to stay zero, minimizations of the EVAM or SLS cost functions can be used to find the kinetic parameters. Minimization can be performed directly by varying k_1, k_2, k_3 and k_4 or by varying parameters k_1, u, v, s and then converting them into k_1, k_2, k_3 and k_4 using expressions (34)–(36). It appears, from several experiments we conducted, that the latter is more efficient in terms of convergence and accuracy in some cases.

The Matlab 6 function 'fmincon' for constrained nonlinear minimization (The MathWorks 2001) was used with the medium-scale optimization option, which employs a sequential quadratic programmingp (SQP) method (The MathWorks 2001). This function allows the specification of boundary as well as nonlinear inequality constraints on the parameters of minimization.

5.1.1. Estimation with the EVAM cost function (three channels). Two-channel $\mathbf{R}$ matrices (Riabkov and DiBella 2002a) were constructed from the three measured TACs, $\mathbf{x}^{(1)}$, $\mathbf{x}^{(2)}$, and $\mathbf{x}^{(3)}$: $\mathbf{R}^{(1,2)}$ from $\mathbf{x}^{(1)}$ and $\mathbf{x}^{(2)}$, $\mathbf{R}^{(1,3)}$ from $\mathbf{x}^{(1)}$ and $\mathbf{x}^{(3)}$, $\mathbf{R}^{(2,3)}$ from $\mathbf{x}^{(2)}$ and $\mathbf{x}^{(3)}$. Eigenvectors $\mathbf{w}^{(1,2)}$, $\mathbf{w}^{(1,3)}$ and $\mathbf{w}^{(2,3)}$, correspondent to the minimal eigenvalues, were calculated from each $\mathbf{R}$ using singular value decomposition. Vectors $\mathbf{p}^{(1,2)}$, $\mathbf{p}^{(1,3)}$, $\mathbf{p}^{(2,3)}$ and $\mathbf{p}^{(2,1)}$, $\mathbf{p}^{(3,1)}$, $\mathbf{p}^{(3,2)}$ were calculated from the corresponding $\mathbf{w}$ that satisfied the following condition,

$$\mathbf{w}^{(i,j)} = \left[w_0^{(i)}\mathbf{p}^{(i,j)T}, w_0^{(j)}\mathbf{p}^{(j,i)T}\right]^T$$

where $w_0^{(i)} = w_0^{(i,j)}$, $w_0^{(j)} = w_4^{(i,j)}$ are the w_0 coefficients of the FIR filters $\mathcal{W}^{(i)}(z)$ and $\mathcal{W}^{(j)}(z)$ of the EVAM blind deconvolution framework for this particular combination of two channels i and j. (Note, for example, that the coefficient $w_0^{(1)}$ for the combination of 1 and 2 channels is not equal to the coefficient $w_0^{(1)}$ for the combination of 1 and 3 channels.) Vectors $\mathbf{p}_e^{(1,2)}$, $\mathbf{p}_e^{(1,3)}$, $\mathbf{p}_e^{(2,3)}$ and $\mathbf{p}_e^{(2,1)}$, $\mathbf{p}_e^{(3,1)}$, $\mathbf{p}_e^{(3,2)}$ were constructed from the u, v, s values such that

$$\mathbf{p}_e^{(i,j)} = \begin{vmatrix} 1 \\ -u^{(i)} - v^{(i)} - s^{(j)} \\ u^{(i)}v^{(i)} + u^{(i)}s^{(j)} + v^{(i)}s^{(j)} \\ -u^{(i)}v^{(i)}s^{(j)} \end{vmatrix}.$$

Then the sum

$$\sum_{i \neq j} \left|\mathbf{p}^{(i,j)} - \mathbf{p}_e^{(i,j)}\right|^2 \qquad (i, j = 1, 2, 3)$$

was minimized by varying u, v and s. The boundary constraints $0 < u, v, s < 1$ were applied during minimization. Because of the arbitrary scale factor α, absolute values of k_1 cannot be estimated by blind identification without additional information. The ratios of k_1 were estimated from $\mathbf{w}$ by

$$\frac{k_1^{(2)}}{k_1^{(1)}} = \frac{w_0^{(1,2)}}{w_4^{(1,2)}} \tag{44}$$

using vector $\mathbf{w}^{(1,2)}$, and

$$\frac{k_1^{(3)}}{k_1^{(1)}} = \frac{w_0^{(1,3)}}{w_4^{(1,3)}} \tag{45}$$

using vector $\mathbf{w}^{(1,3)}$.

5.1.2. Estimation with the SLS cost function (three channels). SLS cost function minimization was done by varying k_1, u, v and s. Gradients of the SLS cost function relative to

k_1, u, v and s were calculated analytically for use with 'fmincon' to speed up the minimization process.

The following constraints were applied during mininimization:

(a) $0 < u < v < s < 1$ from (39);
(b) boundaries for k_1, k_2, k_3, k_4 were specified.

$$\mathbf{k}_{\text{Low}} < \mathbf{k}^{(i)} < \mathbf{k}_{\text{Upp}} \qquad i = 1, 2, 3. \tag{46}$$

If (a) were satisfied than the tighter bounds in (b) were checked. The lower and upper boundaries were implemented by converting u, v, s to k_2, k_3, k_4 during minimization using relations (34)–(36).

5.2. Kinetic parameter estimation—simulation with FDG brain imaging conditions

5.2.1. Description of algorithms. Since SLS has much superior accuracy compared to EVAM, as will be shown in section 5.3, the EVAM cost function was not used in this section.

It is assumed that j-image of the dynamic sequence is acquired during the time interval $[t_j; t_{j+1}]$ where t_j and t_{j+1} are the start and the end of one scan. And the images of the dynamic sequence are taken sequentially, $j = 1, \ldots, N$. The data were assumed to be decay-corrected. Also it is assumed that the measured (simulated) samples of the TAC are in fact average values over the scanning intervals:

$$\text{TAC}_j = \frac{1}{\Delta t_j} \int_{t_j}^{t_{j+1}} \text{TAC}(t)\, \mathrm{d}t$$

where $\Delta t_j = t_{j+1} - t_j$ is the length of the time interval.

The three algorithms used were:

(1) *SLS* (see section 5.1.2);
(2) *Non-uniform sampling SLS (NSLS)*. The FDG blood input is very steep at the origin and very flat at the end. Because of this a modified version of SLS method, which handles non-uniform sampling, was introduced. The modifications are described in appendix A.5.
(3) *Analytical convolution of blood model with tissue response (IFM—input function model)*

To compare the two SLS methods described above with an algorithm modelling the convolution of a blood model (Feng *et al* 1997) with three-compartment tissue responses, the following cost function was minimized,

$$\sum_{i=1}^{3} \sum_{j=1}^{N} \frac{\left|\text{TAC}_j^{(i)} - Q(\mathbf{A}, \boldsymbol{\lambda}, \mathbf{k}^{(i)}, t_j^*)\right|^2}{\sigma_j^{2(i)}}$$

where $\overrightarrow{\text{TAC}} = \vec{x}$ is a measured (simulated) TAC, $Q(t)$ is the model for convolution from equation (74) (see appendix A.7), i is a channel number and t_j^* is the middle of a scan interval $t_j^* = (t_{j+1} + t_j)/2$. The $\sigma_j^{2(i)}$ factor will be described later. This cost function (which will be referred to as the IFM cost function) was minimized by the parameters $\mathbf{A}$, $\boldsymbol{\lambda}$, and $\mathbf{k}^{(1)}$, $\mathbf{k}^{(2)}$, $\mathbf{k}^{(3)}$. Boundary constraints were used for $A_1, A_2, A_3, \lambda_1, \lambda_2, \lambda_3$ according to the specified ranges (see section 5.2.2). Boundary constraints on $k_1, \ldots, k_4$ were applied according to the ranges listed in section 5.2.2.

5.2.2. Conditions. To simulate realistic conditions, the ranges for k were chosen based on the minimum and maximum values found in Huang *et al* (1980), Phelps *et al* (1979) and Feng *et al* (1997).

$$\mathbf{k}_{\text{Low}} = [0.023, 0.048, 0.010, 0.0028]^T \text{ min}^{-1}$$
$$\mathbf{k}_{\text{Upp}} = [0.201, 0.285, 0.096, 0.0098]^T \text{ min}^{-1}.$$

The ranges for A and λ were based on the set of values in Wong *et al* (2001),

$$\mathbf{A}_{\text{Low}} = [851.1/2, 21.9/2, 20.8/2]^T$$
$$\mathbf{A}_{\text{Upp}} = [1510.0, 21.9 \cdot 2, 20.8 \cdot 2]^T$$
$$\boldsymbol{\lambda}_{\text{Low}} = [4.13/3, 0.119/3, 0.0104/3]^T$$
$$\boldsymbol{\lambda}_{\text{Upp}} = [4.13 \cdot 3, 0.119 \cdot 3, 0.0104 \cdot 3]^T.$$

(The value 1510.0 does not fit the pattern because the optimization fails more frequently with $A_{1\,\text{Upp}} = 851.1 \cdot 2$.) The constraints in the algorithms were set according to the intervals shown.

In order to get accuracy estimates true parameter values were simulated with a uniform random distribution in the intervals specified.

The noise model that was used for the TACs is the same as described in Feng *et al* (1997). Noise was generated by a Gaussian distribution with zero mean and the variance σ_j^2 for j-time interval equal to (Feng *et al* 1997)

$$\sigma_j^2 = \frac{\gamma \text{TAC}_j}{\Delta t_j} \tag{47}$$

where γ is a characteristic constant determining the noise level. The noise was then added to the average values of TACs in each time interval.

5.2.3. Time schedules

(1) *SLS*. 450 uniform temporal samples from 0 to 135 min ($\Delta t = 0.3$ min) were used.
(2) *NSLS*. The following non-uniform time schedule was used: 10 samples with Δt of 0.2 min, 10×0.5 min, 10×1 min, 10×1.5 min, 10×3.5 min, 10×5 min (0–117 min). This is more fine than the time schedule in the IFM because the most simple and therefore the least accurate non uniform sampling convolution algorithm was used in SLS.
(3) *IFM*. Temporal samples were taken according to the schedule in Wong *et al* (2001): 10 samples with Δt of 0.2 min, 2×0.5 min, 2×1 min, 1×1.5 min, 1×3.5 min, 2×5 min, 1×10 min, and 3×30 min (0–120 min).

5.2.4. Accuracy estimates. Without noise all of the algorithms gave the exact true solution.

The following scheme was implemented to estimate the accuracy of the three algorithms. N sets of the true $\mathbf{k}$–$\mathbf{A}$–$\boldsymbol{\lambda}$ parameters were simulated. N sets of three TACs were constructed using these parameter sets according to the method described in section 5.2.1 and $Q(t)$. For each of the N noiseless sets of TACs M noisy sets of TACs realizations were generated according to the description in section 5.2.2 with coefficient $\gamma = 0.1$ (such that in (47) Δt is in seconds and TAC is in μCi/ml). N and M were set to 100. An example of three simulated FDG tissue activity curves is shown in figure 3.

Reconstructions of the $\mathbf{k}$ parameters by the three methods (SLS, NSLS and IFM) were performed for each noise realization. The N values of the averages and standard deviations of the $\mathbf{k}$ estimates corresponding to the N true $\mathbf{k}$ were calculated. The relative values of the bias and standard deviation were calculated by dividing values of the bias and standard deviations

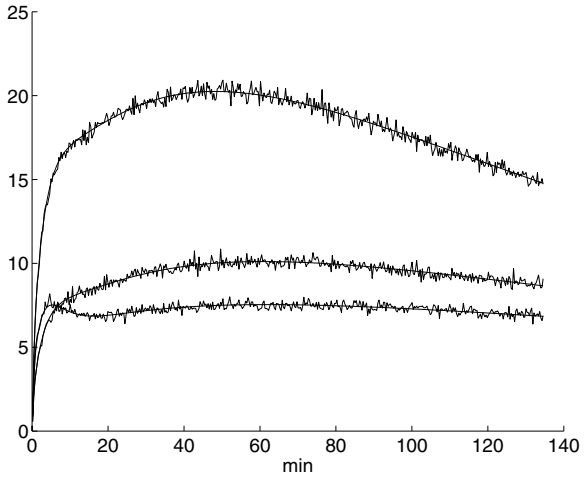

Figure 3. An example of three simulated FDG tissue activity curves used in accuracy estimations (activity in μCi/ml versus time in minutes).

by the true values of the parameters. The calculated relative bias and standard deviations for the three channels were combined into one set since the three true values of **k** for three channels were chosen randomly from the same ranges. Using these biases and standard deviations, distributions for k_2, k_3 and k_4 were obtained (figures 4, 5).

The values of the relative bias and standard deviation were calculated the same way for the ratios of $k_1^{(2)}/k_1^{(1)}$ and $k_1^{(3)}/k_1^{(1)}$ and combined (denoted as $k_1^{(2,3)}/k_1^{(1)}$). Then distributions of the relative bias and standard deviation were calculated (figures 4(a), (b) and 5(a), (b)).

Comparisons of the algorithms are shown in figures 4, 5. The NSLS method shows much better accuracy than uniform SLS for the estimates of the k_1 ratios (figures 4(a), 4(b)). Bias for NSLS k_2 estimates is better than for uniform SLS. However the standard deviation is slightly higher. For k_3 estimates uniform SLS seems to have better accuracy than NSLS. k_4 accuracy is approximately the same for both methods.

NSLS method is less accurate than IFM for k_3 and especially k_4 according to the distributions in figures 5(g) and (h). The accuracy of k_2 estimates is slightly better for IFM. Accuracies for the ratios of k_1 estimates by NSLS and IFM are close to each other. However, some outliers exist in the bias distribution for IFM.

The distributions of the relative bias and standard deviation were calculated for the ratios of $K^{(2,3)}/K^{(1)}$ (figures 6, 7) in similar way as for $k_1^{(2,3)}/k_1^{(1)}$, where the parameter

$$K = \frac{k_1 k_2}{k_2 + k_3} \tag{48}$$

is an important characteristic of the regional glucose metabolism (Phelps *et al* 1979). As can be seen from figure 6, SLS gives better estimates of K ratios than NSLS; however they are close. From figure 7(b) distributions of the relative standard deviations for IFM and SLS are close. However, from figure 7(a) estimates from IFM are less biased than from SLS.

The same conclusions can also be drawn from table 1 which shows means and standard deviations calculated for the distributions presented in figures 4–7. Statistical significance of the comparisons of the means of these distributions was calculated with the t-test (at the $p < 0.05$ significance level) and shown in table 2.

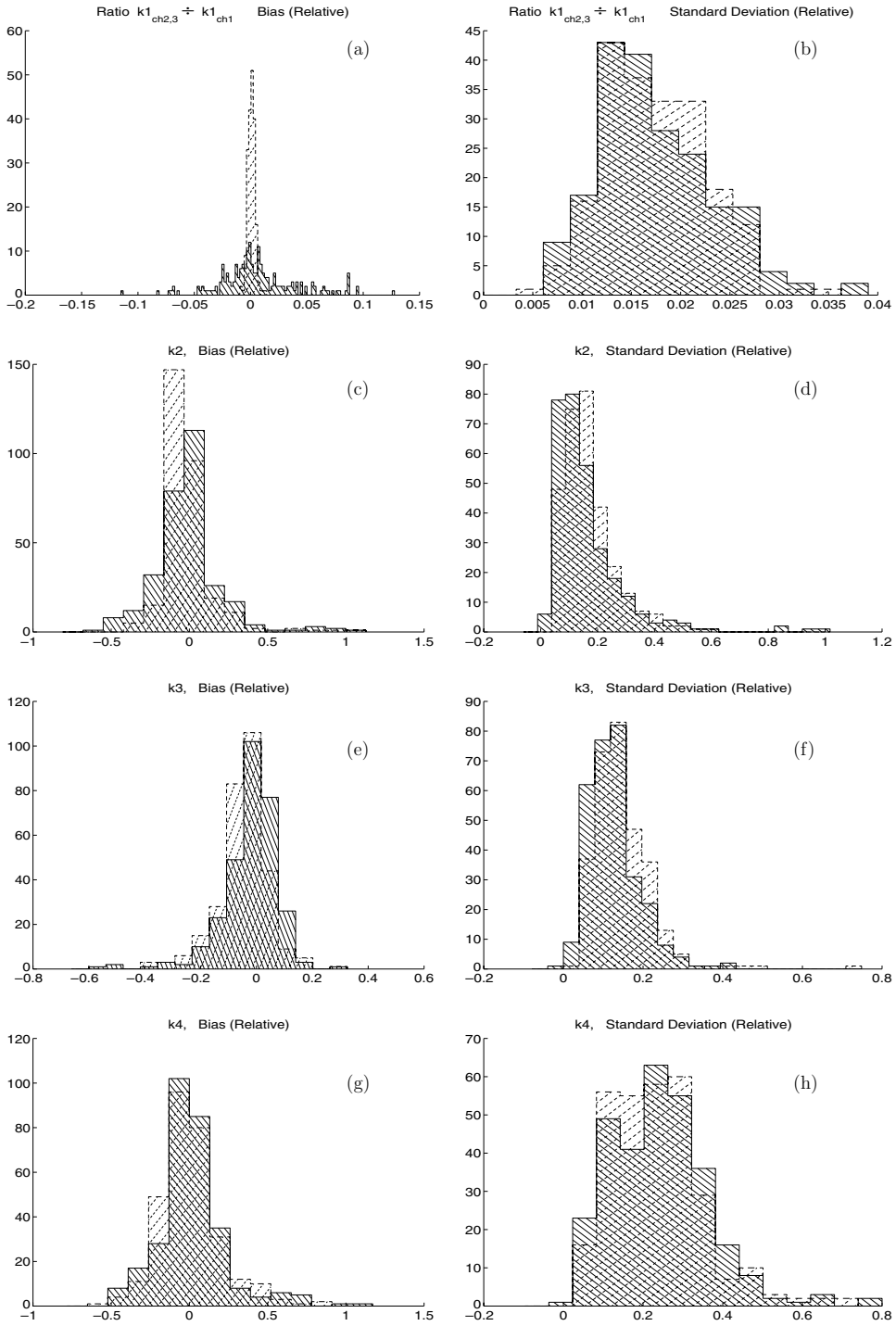

Figure 4. Distributions of relative biases (left column: (a), (c), (e), (g)) and relative standard deviations (right column: (b), (d), (f), (h)) for $k_1^{(2,3)}/k_1^{(1)}$ ((a), (b)) and k_2 ((c), (d)), k_3 ((e), (f)), k_4 ((g), (h)) estimates by SLS (solid) and NSLS (dash) methods computed from simulated noisy TACs.

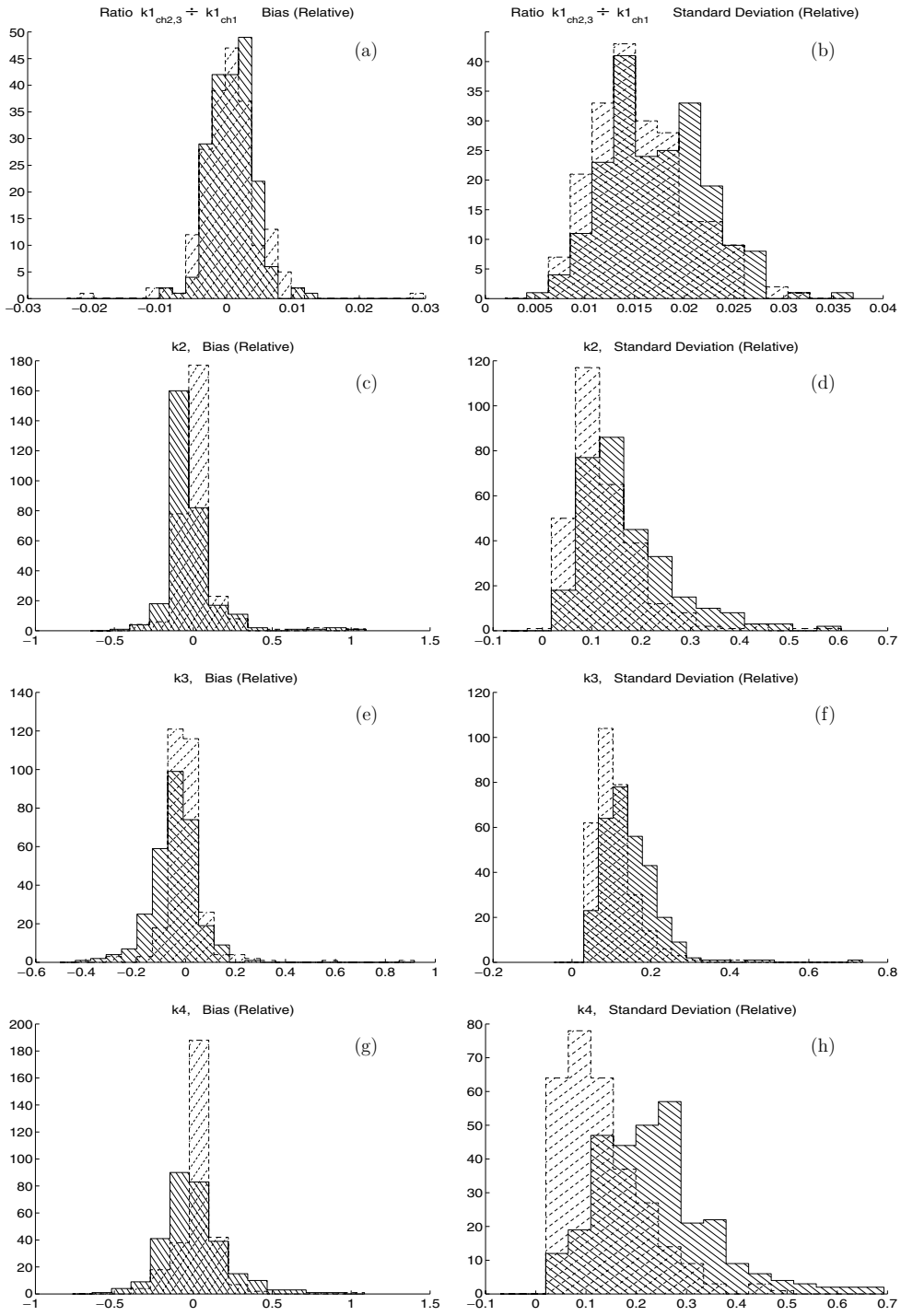

Figure 5. Distributions of relative biases (left column: (a), (c), (e), (g)) and relative standard deviations (right column: (b), (d), (f), (h)) for $k_1^{(2,3)}/k_1^{(1)}$ ((a), (b)) and k_2 ((c), (d)), k_3 ((e), (f)), k_4 ((g), (h)) estimates by NSLS (solid) and IFM (dash) methods computed from simulated noisy TACs.

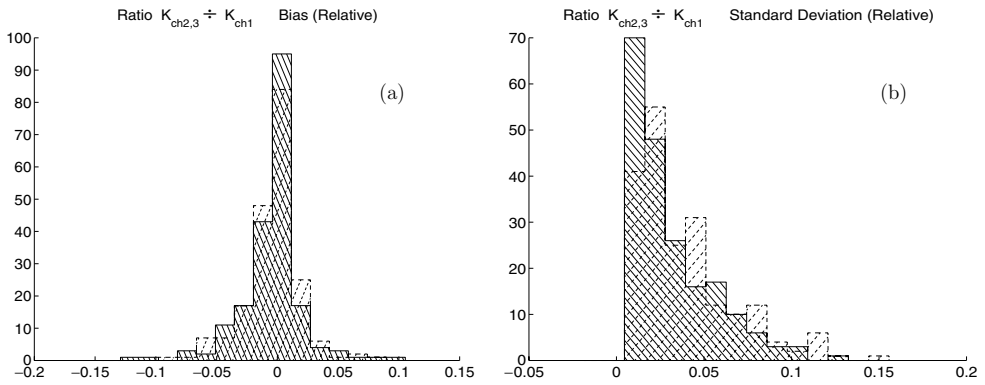

Figure 6. Distributions of relative biases (a) and relative standard deviations (b) for $K^{(2,3)}/K^{(1)}$ estimates by SLS (solid) and NSLS (dash) methods computed from simulated noisy TACs.

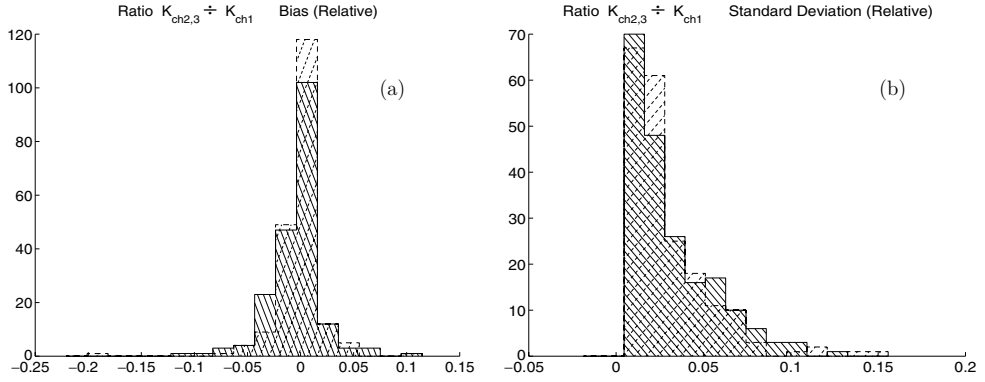

Figure 7. Distributions of relative biases (a) and relative standard deviations (b) for $K^{(2,3)}/K^{(1)}$ estimates by SLS (solid) and IFM (dash) methods computed from simulated noisy TACs.

5.3. Kinetic parameter estimation—simulation with fewer sample points and different conditions

Different sets of tissue activity curves were simulated to check the feasibility of the blind identification algorithms for the three-compartment system at some different conditions. The following conditions were used in the simulations.

A rapid input curve (shown in figure 8) was taken as the blood input for these simulations. Forty-nine time frames were used. The time interval between frames was 2 s. Boundaries for the kinetic parameters were specified as

$$\mathbf{k}_{\mathrm{Low}} = [1, 1, 1, 1]^T \qquad \mathbf{k}_{\mathrm{Upp}} = [12, 12, 12, 12]^T$$

in min^{-1}. Kinetic parameters k_1, k_2, k_3, k_4 were randomly selected integer values from the intervals specified by the boundaries $[\mathbf{k}_{\mathrm{Low}}; \mathbf{k}_{\mathrm{Upp}}]$ to generate TACs for three channels.

Additive Gaussian white noise was introduced into the simulated tissue activity curves. Several different variances for the noise corresponding to the SNR in TACs starting from 10^1 to higher SNR were tried.

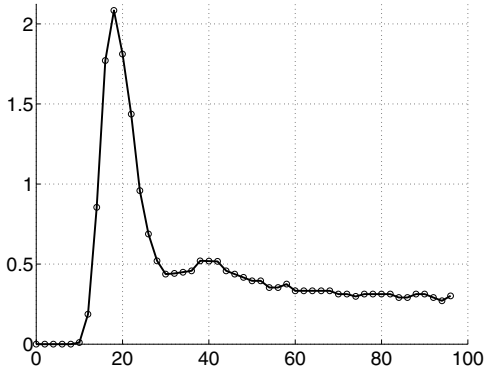

Figure 8. Blood input function (concentration in arbitrary units versus time in seconds).

Table 1. Means and standard deviations (in %) of the distributions in figures 4–7: *b*—distributions of relative biases, *s*—distributions of relative standard deviations.

		SLS		NSLS		IFM	
		Mean	Std	Mean	Std	Mean	Std
$k_1^{(2,3)}/k_1^{(1)}$	*b*	0.6	3.5	0.08	0.32	0.05	0.46
	s	1.7	0.6	1.7	0.5	1.6	0.5
k_2	*b*	−1	22	−1	16	1	13
	s	16	13	17	9	13	8
k_3	*b*	−2	10	−4	9	−0.08	9.05
	s	13	6	15	7	11	5
k_4	*b*	2	22	0.3	19.9	2	12
	s	24	12	24	12	13	8
$K^{(2,3)}/K^{(1)}$	*b*	−0.4	2.5	−0.3	2.3	−0.1	2.2
	s	3.2	2.3	3.9	2.8	2.9	2.4

Table 2. Statistical significance of the comparisons of the means of the distributions in figures 4–7 with *t*-test (at the $p < 0.05$ significance level): H_0 hypothesis, that the means of the two distributions are equal, is accepted (denoted by +) or rejected (denoted by −). The distributions: *b*—distributions of relative biases, *s*—distributions of relative standard deviations.

		SLS and NSLS	NSLS and IFM	SLS and IFM
$k_1^{(2,3)}/k_1^{(1)}$	*b*	+	+	+
	s	+	−	−
k_2	*b*	+	+	+
	s	+	−	−
k_3	*b*	−	−	−
	s	−	−	−
k_4	*b*	+	+	+
	s	+	−	−
$K^{(2,3)}/K^{(1)}$	*b*	+	+	+
	s	−	−	+

5.3.1. Using the EVAM cost function. For the noiseless cases the resultant values were exact matches of the input values and unique solutions were reached. In the cases with added noise, the same algorithm was not robust even for high SNR up to 10^7.

5.3.2. Using the SLS cost function. Compared to EVAM, the SLS cost function is more sensitive to the parameters so it can give better accuracy for their estimates. However, since the SLS cost function is more sensitive, it is more difficult to find the global minimum. Because of that, minimizations were performed not only by 'fmincon' but also by simulated annealing (SA), which is an algorithm for global minimization. A simulated annealing function was converted from Fortran (program by B Goffe (Goffe *et al* 1994)) to Matlab. Constraints for the SA function were implemented by setting the cost function to a very large value when the constraint requirement is not satisfied at the current combination of the varying parameters.

The value of the SLS cost function for the true solution was calculated. This value corresponds to the global minimum in the noiseless case and very close to it if the noise is small. The value of the cost function reached in the result of the minimization was compared with the value at the global minimum in order to tell whether the global solution was reached or if the minimization had gotten stuck at a local minimum.

Even in the case without noise, both minimization functions, 'fmincon' and SA, found the global minimum only occasionally. They tended to get stuck at local minima. However, the values of the cost function at these local minima were close to the value at the global minimum. Several minimizations were tried from different starting estimates for the u, v, s parameters. Those minimizations converged to similar but different values.

The solution to this global minimum-finding problem (which was not an issue with more standard FDG parameters in section 5.2) was found by minimizing the logarithm of the SLS cost function instead of the SLS cost function itself. This modification allowed convergence of the algorithm to the exact true solution in the noiseless case. In the case of noisy TACs, this modified algorithm was always able to find the global minimum solution. Minimizations from different starting values converged to the same global minimum. This result was observed for about 10 different realizations of $k_1, \ldots, k_4$, and different noise realizations.

However, it became clear that the presence of noise shifts the global minimum from the true solution. This shift for the SLS cost function seems to be smaller than for EVAM. As predicted, the convergence of SLS on the true solution was observed in the presence of significantly higher noise (at SNR of about 3×10^2) than for EVAM. Minimizations with the SA program improved the accuracy slightly, however they were much slower than minimizations performed by 'fmincon'.

Without the constraint (46) 'fmincon' would not work at all. It would tend to put all u, v, s to 0 and then cause machine exceptions such as division by zero. Constraints, especially (46), were very beneficial in the sense that they noticeably reduced the number of minima corresponding to the false solutions in which cost function could have fallen.

Minimization of the logarithm of the SLS cost function using $k_1, \ldots, k_4$ yields the same results described above. However, it converges from 3 to 10 times slower, and sometimes gives accuracy worse than minimization by varying u, v, s.

6. Discussion and conclusions

Three channels or more should be used to avoid the possibility of non-unique solutions. The blind identification methods (SLS and EVAM) work for the three-compartment model at many

conditions in the case of three or more channels. As discussed above, if there is a problem of finding the global minimum, minimization of the logarithm of the SLS cost function may be helpful.

With EVAM we were able to show that the identification of parameters in the noiseless case for three or more channels can be done by tracing which of the three roots for each channel repeats itself in solutions for all pair combinations of any channel with this particular channel. However, this method is not acceptable in the case when noise is not zero. While it is a very good analytical tool, EVAM gives large errors with noisy data.

EVAM requires the channel transfer functions not to have common poles or zeros while SLS only requires the channel transfer functions to be different. The first requirement is more rigorous than the second. Therefore it can be violated (or close to violated) more easily, which can also be a cause of instability in EVAM.

For the estimates of K ratios, the SLS method gave better accuracy than NSLS, and the performance of SLS is comparable to IFM. SLS or NSLS are likely better choices if the input model is not known exactly. For all of the methods, the k_1 and K ratio estimates are more stable than the estimates of the other parameters. The variability of k_1 is smaller than the other parameters because it is just a scale factor for the curves, the other parameters are all modifying the shape of the curve which is very nonlinear problem and apparently there are many combinations of k_2, k_3, k_4 which produce close curve shapes.

NSLS is much faster than SLS because of the smaller number of samples in FDG brain imaging conditions. Also in the initial work we tried three different time schedules and found that their accuracy varied. The schedule that most accurately reperesented the TACs was used here, but further optimization may improve the NSLS results.

Minimization of the SLS cost function is more efficient by u, v, s parameters than by $\mathbf{k}$ timewise and probably in terms of accuracy.

A case with conditions much different from FDG was investigated in section 5.3. These conditions are similar to those used in a three-compartment model for the gadolinium-DTPA in infarcted myocardium (Moran *et al* 2002). Blind identification was possible for these types of conditions, with very high SNR beyond that which is practical, with a modified SLS technique. A modified SLS technique was used because a global minimum is difficult to find since the SLS cost function in the three-compartment case has many local minima and/or the convex area around the global minima is very small. The results of minimization showed that the logarithm of the SLS cost function may improve finding the global minimum. Constraints are beneficial for decreasing the number of the local minima.

Appendix

A.1. Roots

Define the following constants,

$$U = \frac{n_2}{3} - \frac{n_1^2}{9} \qquad F = \frac{\left(36n_2n_1 - 108n_3 - 8n_1^3 + 12\sqrt{G}\right)^{1/3}}{6}$$

where

$$G = 12n_2^3 - 3n_2^2n_1^2 - 54n_2n_1n_3 + 81n_3^2 + 12n_3n_1^3 \qquad L = F - \frac{U}{F} \qquad V = F + \frac{U}{F}$$

then the roots (no ordering) of the $p(z)$ polynomial are

$$r_1 = L - \frac{n_1}{3} \tag{49}$$

$$r_2 = -\frac{L}{2} + \frac{\mathrm{i}V\sqrt{3}}{2} - \frac{n_1}{3} \tag{50}$$

$$r_3 = -\frac{L}{2} - \frac{\mathrm{i}V\sqrt{3}}{2} - \frac{n_1}{3}. \tag{51}$$

A.2. Kinetic parameters

Suppose that we have found u, v and s for some channel. Then due to equations (37) the coefficients a_1 and a_2 are known. Let us find k_2, k_3 and k_4. From the system of equations (9) and (10)

$$\begin{cases} a_1 = \dfrac{k_2 + k_3 + k_4 - q}{2} \\ a_2 = \dfrac{k_2 + k_3 + k_4 + q}{2} \end{cases} \tag{52}$$

it follows that

$$\begin{cases} a_1 + a_2 = k_2 + k_3 + k_4 \\ (a_2 - a_1)^2 = q^2. \end{cases} \tag{53}$$

Then from (11)

$$q = \sqrt{(k_2 + k_3 + k_4)^2 - 4k_2k_4} \qquad (a_2 - a_1)^2 = (a_1 + a_2)^2 - 4k_2k_4 \tag{54}$$

we have

$$k_4 = \frac{a_2a_1}{k_2} \tag{55}$$

and

$$k_3 = -k_2 + (a_1 + a_2) - \frac{a_2a_1}{k_2}. \tag{56}$$

To find k_2 we will use the fact that we know s, and we will also use relationship (18)

$$c_1 = -B_1v + B_2u.$$

From expression (8)

$$B_1 = \frac{k_1}{q}(k_3 + k_4 - a_1) \qquad B_2 = \frac{k_1}{q}(k_3 + k_4 - a_2)$$

and expressions (53)

$$k_3 + k_4 = a_1 + a_2 - k_2 \tag{57}$$

it follows that B_1 and B_2 are equal to

$$B_1 = \frac{k_1}{q}(a_2 - k_2) \tag{58}$$

$$B_2 = \frac{k_1}{q}(a_1 - k_2). \tag{59}$$

So we can write the expression

$$c_1 = \frac{k_1}{q}[-(a_2 - k_2)v + (a_1 - k_2)u] \tag{60}$$

from which it follows that k_2 is given by

$$k_2 = \frac{c_1(a_2 - a_1)/k_1 + va_2 - ua_1}{v - u} \tag{61}$$

$$k_2 = \frac{-s(a_2 - a_1) + va_2 - ua_1}{v - u}. \tag{62}$$

A.3. Tissue response

By substituting expression (36) for k_2 into formula (58) for B_1, it can be verified using the relation $q = a_2 - a_1$ that

$$B_1 = k_1 \frac{u - s}{u - v} \tag{63}$$

and by substituting into formula (59) for B_2 that

$$B_2 = -k_1 \frac{s - v}{u - v}. \tag{64}$$

Therefore the tissue response (7) can be written as

$$h(n) = \frac{k_1}{u - v}((u - s)u^n + (s - v)v^n). \tag{65}$$

A.4. Intervals for poles and zeros

This section shows that

$$0 < v < s < u < 1. \tag{66}$$

It is assumed that all rates $k_1, k_2, k_3, k_4 > 0$.
(1) Let us show that

$$0 < v < u < 1.$$

Proof. It follows from (9) and (11) that

$$a_1 > 0$$

and from (10) and (11) that

$$a_2 > 0.$$

Then from (13)

$$u \text{ and } v \in]0; 1[. \tag{67}$$

Also from (9)–(11) it follows that $a_1 < a_2$, then from (13)

$$v < u.$$

□

(2) Let us show that

$$v < s < u.$$

Proof. From (18) we have

$$c_1 = -B_1 v + B_2 u$$

from (23) it follows that

$$s = -\frac{c_1}{k_1} = \frac{B_1 v - B_2 u}{k_1}. \tag{68}$$

From (8) and (10), we have

$$B_2 = \frac{k_1}{q} \frac{(k_3 + k_4 - k_2 - q)}{2} \tag{69}$$

and from (8) and (9),

$$B_1 = \frac{k_1}{q}\frac{(k_3 + k_4 - k_2 + q)}{2}. \tag{70}$$

Then

$$s = \frac{v(k_3 + k_4 - k_2 + q) - u(k_3 + k_4 - k_2 - q)}{2q} \qquad s = \frac{v+u}{2} + \frac{v-u}{2}\left[\frac{k_3 + k_4 - k_2}{q}\right].$$

Therefore if

$$-1 < \frac{k_3 + k_4 - k_2}{q} < 1$$

it follows that

$$v < s < u.$$

□

(3) Let us show that

$$-1 < \frac{k_3 + k_4 - k_2}{q} < 1. \tag{71}$$

Proof. From (11)

$$\begin{aligned} q^2 &= (k_2 + k_3 + k_4)^2 - 4k_2k_4 \\ &= (k_2 + k_4)^2 - 4k_2k_4 + 2k_3(k_2 + k_4) + k_3^2 \\ &= (k_2 - k_4)^2 + 2k_3(k_2 + k_4) + k_3^2. \end{aligned}$$

Also

$$(k_3 + k_4 - k_2)^2 = (k_4 - k_2)^2 + 2k_3(k_4 - k_2) + k_3^2.$$

Then

$$(k_3 + k_4 - k_2)^2 < q^2 \qquad \frac{(k_3 + k_4 - k_2)^2}{q^2} < 1.$$

Therefore

$$\left|\frac{k_3 + k_4 - k_2}{q}\right| < 1.$$

□

A.5. Non-uniform sampling SLS

Assume there are N time intervals during which N images were acquired. We denote $[t_p; t_{p+1}]$ as the p-interval starting at t_p and ending at t_{p+1} where $p = 1, \ldots, N$. Then the following time schedule vector can be formed as

$$\mathbf{t} = [t_1, \ldots, t_N, t_{N+1}]^T.$$

For channel e, the tissue response vector $\mathbf{h}$, the tissue activity curve $\vec{x} = \overrightarrow{\mathrm{TAC}}$ and the blood input $\mathbf{b}$ can be defined as follows:

$$\mathbf{h}^{(\mathrm{e})} = [h_1, \ldots, h_N]^T \qquad \vec{x}^{(\mathrm{e})} = \left[x_1^{(\mathrm{e})}, \ldots, x_N^{(\mathrm{e})}\right]^T \qquad \mathbf{b} = [b_1, \ldots, b_N]^T$$

where elements h_p, $x_p^{(\mathrm{e})}$ and b_p are defined at the time $(t_p + t_{p+1})/2$. Also in order to build the SLS linear system, elements of the convolution matrix $\mathbf{H}^{(\mathrm{e})}$

$$H(q, p) \qquad q, p = 1, \ldots, N$$

need to be redefined (here q denotes row and p denotes column) so that the relation

$$\vec{x}^{(e)} = \mathbf{H}^{(e)}\mathbf{b} \tag{72}$$

will be still valid with the new temporal sampling. For $p > q$, $H(q, p) = 0$ for $p \leqslant q$, then the value of $H(q, p)$ will have to be determined.

Define the following auxiliary time schedule vector for each q,

$$\mathbf{v}_q = t_{q+1} - [t_{q+1}, \ldots, t_1]^T.$$

We look for the maximum a in $a = 1, \ldots, q$ such that

$$v_{q,a} < t_p$$

and for minimum b in $b = 1, \ldots, q$ such that

$$t_{p+1} \leqslant v_{q,b}.$$

Let us define another vector, a vector of weights $\tau_{p,q}$ of some length M with two possibilities:

(1) If a is equal to $b - 1$ (p—interval is inside of interval a of time schedule $\mathbf{v}_q$), then

$$M = 1 \qquad \tau_{p,q,1} = t_{p+1} - t_p.$$

(2) If a is not equal to $b - 1$, then

$$M = b - a \qquad \tau_{p,q,1} = v_{q,a+1} - t_p \qquad \tau_{p,q,M} = t_{p+1} - v_{q,b-1}.$$

Also, if $a + 1$ is not equal to $b - 1$ (i.e. $M > 2$) then

$$\tau_{p,q,c+1} = v_{q,a+1+c} - v_{q,a+c} \qquad c = 1, \ldots, M - 2.$$

Then for $p \leqslant q$ the approximation to the element $H(q, p)$ can be defined as

$$H(q, p) = \sum_{i=1}^{M} \tau_{p,q,i} h_{q+1-(a(p,q)+i-1)}$$

and equation (72) would hold approximately. Note that the approximation is more exact when the time intervals are smaller.

The tissue response h_i at the moment $t_n = (t_i + t_{i+1})/2$ is calculated as $h(n)$ in formula (38), but $n = t_n/\Delta t$. While single Δt does not exist for this nonuniform sampling case, we can choose an arbitrary Δt and use it to define u, v, s (13), (23). (We used $\Delta t = 0.3$ min.) It also should be used in formulae (37) for a_1 and a_2 needed for conversion of u, v, s to k_2, k_3, k_4.

A.6. FDG blood input model

The blood input function model described in Feng *et al* (1997) for FDG brain PET was used:

$$b(\mathbf{A}, \boldsymbol{\lambda}, t) = (A_1 t - A_2 - A_3)\,\mathrm{e}^{-\lambda_1 t} + A_2\,\mathrm{e}^{-\lambda_2 t} + A_3\,\mathrm{e}^{-\lambda_3 t} \tag{73}$$

where

$$\mathbf{A} = [A_1, A_2, A_3]^T \qquad \boldsymbol{\lambda} = [\lambda_1, \lambda_2, \lambda_3]^T.$$

Values of the coefficients $A_1 = 851.1225\,(\mu\mathrm{Ci\ ml^{-1}\ min^{-1}})$, $A_2 = 21.8798\,(\mu\mathrm{Ci\ ml^{-1}})$, $A_3 = 20.8113\,(\mu\mathrm{Ci\,ml^{-1}})$, $\lambda_1 = 4.1338\,(\mathrm{min^{-1}})$, $\lambda_2 = 0.1191\,(\mathrm{min^{-1}})$, $\lambda_3 = 0.0104\,(\mathrm{min^{-1}})$ are given in Feng *et al* (1997) for a typical FDG blood input curve.

A.7. FDG TACs model

The analytical expression for the convolution of the FDG tissue response (7) with the input function (73) was derived for this work which can be written as follows:

$$Q(\mathbf{A}, \boldsymbol{\lambda}, \mathbf{k}, t) = (h \otimes b)(t) = B_1 G_1 \, \mathrm{e}^{-a_1 t} - B_2 G_2 \, \mathrm{e}^{-a_2 t} + (B_1 E_1 - B_2 E_2) \, \mathrm{e}^{-\lambda_1 t} + T_2 \, \mathrm{e}^{-\lambda_2 t} + T_3 \, \mathrm{e}^{-\lambda_3 t} \tag{74}$$

where

$$G_1 = \frac{A_1/f_1 + U}{f_1} - y_{21} - y_{31} \qquad G_2 = \frac{A_1/f_2 + U}{f_2} - y_{22} - y_{32}$$

$$E_1 = \frac{(A_1(t - 1/f_1) - U)}{f_1} \qquad E_2 = \frac{(A_1(t - 1/f_2) - U)}{f_2}$$

and

$$U = A_2 + A_3 \qquad f_1 = a_1 - \lambda_1 \qquad f_2 = a_2 - \lambda_1$$

$$y_{31} = \frac{A_3}{(a_1 - \lambda_3)} \qquad y_{32} = \frac{A_3}{(a_2 - \lambda_3)}$$

$$y_{21} = \frac{A_2}{(a_1 - \lambda_2)} \qquad y_{22} = \frac{A_2}{(a_2 - \lambda_2)}$$

$$T_3 = y_{31} B_1 - y_{32} B_2 \qquad T_2 = y_{21} B_1 - y_{22} B_2.$$

References

Bresler Y and Macovski A 1986 Exact maximum likelihood parameter estimation of superimposed exponential signals in noise *IEEE Trans. Audio, Speech, Signal Process.* **34** 1081–9

Chen K, Bandy D, Reiman E, Huang S-C, Lawson M, Feng D, Yun L and Palant A 1998 Noninvasive quantification of the cerebral metabolic rate for glucose using positron emission tomography ^{18}F-Fluoro-2-Deoxyglucose, the Patlak method, and an image derived input function *J. Cereb. Blood Flow Metab.* **18** 716–23

DiBella E V R, Clackdoyle R and Gullberg G T 1999 Blind estimation of compartmental model parameters *Phys. Med. Biol.* **44** 765–80

Feng D, Wong K-P, Wu C-M and Siu W 1997 A technique for extracting physiological parameters and the required input function simultaneously from PET image measurements: theory and simulation study *IEEE Trans. Inform. Technol. Biomed.* **1** 243–54

Goffe W L, Ferrier G D and Rogers J 1994 Global optimization of statistical functions with simulated annealing *J. Econometrics* **60** 65–100

Golub G H and Pereyra V 1973 The differentiation of pseudo-inverses and nonlinear least squares problems whose variables separate *SIAM J. Numer. Anal.* **10** 413–32

Gürelli M I and Nikias C L 1995 EVAM: an eigenvector-based algorithm for multichannel blind deconvolution of input colored signals *IEEE Trans. Signal Process.* **43** 134–49

Huang S-C, Phelps M E, Hoffman E J, Sideris K, Selin C J and Kuhl D E 1980 Noninvasive determination of local cerebral metabolic rate of glucose in man *Am. J. Physiol.* **238** E69–82

Moran G R, Thornhill R E, Sykes J and Prato F S 2002 Myocardial viability imaging using Gd-DTPA: physiological modelling of infarcted myocardium, and impact on injection strategy and imaging time *Magn. Reson. Med.* **48** 791–800

Phelps M E, Huang S C, Hoffman E J, Selin C J, Sokoloff L and Kuhl D E 1979 Tomographic measurement of local cerebral glucose metabolic rate in humans with (F-18)2-fluoro-2-deoxy-D-glucose: validation method *Ann. Neuro.* **6** 371–88

Proakis J G and Manolakis D G 1996 *Digital Signal Processing: Principles, Algorithms and Applications* 3 edn (Upper Saddle River, NJ: Prentice-Hall)

Riabkov D Y and DiBella E V R 2002a Estimation of kinetic parameters without input functions: analysis of three methods for multichannel blind identification *IEEE Trans. Biomed. Eng.* **49** 1318–27

Riabkov D Y and DiBella E V R 2002b Theoretical analysis of blind identification of kinetic parameters in a three compartment model: nonuniqueness problem *IEEE Int. Symp. Biomed. Imag. Proc. (Washington, DC, 7–10 July 2002)* pp 581–5

Takikawa S, Dhawan V, Spetsieres P, Robeson W, Chaly T, Dahl R, Margouleff D and Eidelberg D 1993 Noninvasive quantitative fluorodeoxyglucose PET studies with an estimated input function derived from a population-based arterial blood curve *Radiology* **188** 131–6

The MathWorks 2001 *Matlab Optimization Toolbox User's Guide (Matlab 6, Release 12.1)* (Natick, MA: The MathWorks)

Tong L and Perreau S 1998 Multichannel blind identification: from subspace to maximum likelihood methods *Proc. IEEE* **86** 1951–68

Wong K-P, Feng D, Meikle S R and Fulham M J 2001 Simultaneous estimation of physiological parameters and the input function—*in vivo* PET data *IEEE Trans. Inform. Technol. Biomed.* **5** 67–76